C. R. Chimie 22 (2019) 327–336

Contents lists available at ScienceDirect

Comptes Rendus Chimie

www.sciencedirect.com

Full paper/Mémoire

Preparation and characterization of $H_{3-2(x+y)}Mn_xCo_yPMo_{12}O_{40}$ heteropolysalts. Application to adipic acid green synthesis from cyclohexanone oxidation with hydrogen peroxide

Préparation et caractérisation des hétéropolysels $H_{3-2(x+y)}Mn_xCo_yPMo_{12}O_{40}$. Application à la synthèse verte de l'acide adipique par oxydation de la cyclohexanone avec du peroxyde d'hydrogène

Sihem Mouanni [a], Tassadit Mazari [a, b, *], Dahbia Amitouche [a, b], Sihem Benadji [a], Leila Dermeche [a, b], Catherine Roch-Marchal [c], Chérifa Rabia [a]

[a] *Laboratoire de chimie du gaz naturel, Faculté de chimie, USTHB, BP32, El-Alia, 16111 Bab-Ezzouar, Alger, Algeria*
[b] *Laboratoire de chimie appliquée et de génie chimique, Université Mouloud-Mammeri (UMMTO), Tizi-Ouzou, Algeria*
[c] *ILV—UMR 8180 CNRS, Bâtiment Lavoisier, Université de Versailles-Saint-Quentin-en-Yvelines, 45, avenue des États-Unis, 78035 Versailles cedex, France*

ARTICLE INFO

Article history:
Received 8 June 2018
Accepted 14 January 2019
Available online 22 February 2019

Keywords:
Cobalt- and manganese-substituted Keggin mixed salt
Cyclohexanone oxidation
Hydrogen peroxide
Adipic acid

ABSTRACT

$H_{3-2(x+y)}Mn_xCo_yPMo_{12}O_{40}$ heteropolysalts ($x + y \leq 3/2$ and x, y: 0–1.5) were prepared by a cationic exchange method based on barium sulfate precipitation. Structural and textural properties of salts were examined by several physicochemical techniques such as infrared, scanning electron microscopy-energy dispersive X-ray, and ^{31}P nuclear magnetic resonance spectroscopies, X-ray diffraction diffraction, and thermogravimetric analysis, and their catalytic properties were evaluated in the cyclohexanone oxidation using hydrogen peroxide (30%). The reaction products, adipic, glutaric, succinic, hexanoic, 6-hydroxyhexanoic, 7,7-dimethoxy, and heptanoic acids and 1,1-dimethoxy octane were identified by gas chromatography—mass spectrometry analysis. Only adipic, glutaric, and succinic acids were quantified by chromatography (high-performance liquid chromatography), the other products were noted X. Adipic acid (AA) is the major product for all systems. The effects of molar ratios of catalyst/reactant and cyclohexanol/cyclohexanone, heteropolysalt composition, and reaction duration on AA yield were investigated. The stability of the catalytic system was also examined. $H_{3-2(x+y)}Mn_xCo_yPMo_{12}O_{40}$ catalysts were found to be efficient for the cyclohexanone oxidation with conversions >95%. Among them, $H_1Mn_{0.25}Co_{0.75}$ exhibits the highest AA yield (75%).

* Corresponding author.
E-mail address: tassa2002@gmail.com (T. Mazari).

https://doi.org/10.1016/j.crci.2019.01.003
1631-0748/

Mots clés:
Cobalt
Phosphomolybdates de manganèse
Oxydation de la cyclohexanone
Peroxyde d'hydrogène
Acide adipique

RÉSUMÉ

Les hétéropolysels $H_{3-2(x+y)}Mn_xCo_yPMo_{12}O_{40}$ ($x + y \leq 3/2$ et x, y: 0–1,5) ont été préparés par une méthode d'échange cationique basée sur la précipitation du sulfate de baryum. Les propriétés structurales et texturales des sels ont été examinées par plusieurs techniques physico-chimiques telles que les spectroscopies IR, MEB/EDX et RMN ^{31}P, la diffraction des rayons X et l'analyse TG. Leurs propriétés catalytiques ont été évaluées dans l'oxydation de la cyclohexanone en utilisant le peroxyde d'hydrogène (30%). Les produits de la réaction, acides adipique, glutarique, succinique, hexanoïque, 6-hydroxyhexanoïque, 7,7-diméthoxy, heptanoïque et 1,1-diméthoxy octane, ont été identifiés par analyse GC-MS. Seuls les acides adipique, glutarique et succinique ont été quantifiés par chromatographie (HPLC), les autres produits ont été notés X. L'acide adipique (AA) est le principal produit de la réaction. Les effets des rapports molaires catalyseur/réactif et cyclohexanol/cyclohexanone, de la composition du sel et du temps de réaction sur le rendement en AA ont été étudiés. La stabilité du système catalytique a également été examinée. Les catalyseurs $H_{3-2(x+y)}Mn_xCo_yPMo_{12}O_{40}$ se sont révélés être efficaces pour l'oxydation de la cyclohexanone avec des conversions >95%. Parmi eux, $H_1Mn_{0.25}Co_{0.75}$ conduit au rendement le plus élevé en AA (75%).

1. Introduction

One of the major drawbacks in the actual adipic acid (AA) production process is the N_2O emission [1–3]. It is one of the ozone depleting agents with a strong greenhouse effect and a very long residence time in the atmosphere, thus leading to serious environmental problems [4,5].

AA is an important raw material for nylon-6,6 production [6,7] and other compounds as synthetic fibers and fine chemicals [1]. It is usually produced via the oxidation of a mixture of cyclohexanone and cyclohexanol (KA oil) in the presence of an excess of HNO_3 (40–60%) using Cu^{II}/NH_4VO_3 as a catalyst [1,5]. The HNO_3 reduction causes inevitably the release of nitrous oxides (N_2O, NO, and NO_2), which are harmful gases. Others powerful oxidants as $Na_2Cr_2O_7$, NaClO, MnO_2, $KMnO_4$ are cited in the literature [8–14], but they are noxious too. Therefore, the development of a process that would belong to the "green chemistry" domain is more than necessary. So, several studies have focused on the search for benign oxidants for environment as H_2O_2, O_2, and air. Among them, hydrogen peroxide is the most used, easier to handle, and moreover, its reduction leads only to water. It was used for KA oil production from cyclohexane oxidation using transition metal based catalysts as Cu/Cr_2O_3 [15], $CoFe_2O_4$ [16], Co_3O_4 [17], $Ce_{1-x}Mn_xO_2$ [18], Cu/Co/AC [19], WO_3/V_2O_5 [20], HMS [21], MCM-48 [22], Cu/Cr_2O_3, AlPO-5 modified with rare earth elements [23,24], and A-HMS (A = Ce, Ti, Co, Al, Cr, V, and Zr) [21] and MnAlPO [25]. It was found that the most effective systems for cyclohexane oxidation are those based on Mn and Co elements [26,27].

Furthermore, polyoxometalates (POMs) have received great attention in the catalysis field because of their multifunctional properties. They were extensively studied for various reactions as olefin epoxidation [28], organosilane oxidation [29], organic pollutant photo-oxidative degradation [30], oxidation of alcohols [31–33], cyclohexane [34,35], and cyclohexanol/cyclohexanone [36–40]. In this last case, the examined catalytic systems are $M_xPMo_{12}O_{40}$ (M = Fe, Ni, Co and x = 1 or 1.5) [36], $H_{3-2x}Ni_xPMo_{12}O_{40}$ and $(NH_4)_{3-2x}Ni_xPMo_{12}O_{40}$ [37], $(NH_4)_xA_yPMo_{12}O_{40}$ (A^{n+} = Sb^{3+}, Bi^{3+}, or Sn^{2+}) [38], $H_{3-2x}Co_xPMo_{12}O_{40}$ (x: 0–1.5) [39], and α2-$K_6P_2Mo_5W_{13}O_{62}$, α-$K_6P_2Mo_6W_{12}O_{62}$, and α1-$K_7P_2Mo_5VW_{12}O_{62}$ [40]. They showed high activities and led to high AA yields. Seventy percent of AA yield was attained with α-$K_6P_2Mo_6W_{12}O_{62}$ from the mixture of ol/one oxidation.

On the basis of the literature highlighting the efficiency of Mn- and Co-based catalysts for the oxidation of cyclohexane, in this study, we propose to introduce these two elements as counterion of $[PMo_{12}O_{40}]^{3-}$. So, a series of POMs of formula $H_{3-2(x+y)}Mn_xCo_yPMo_{12}O_{40}$, noted $H_{3-2(x+y)}Mn_xCo_y$ ($x + y \leq 3/2$ and x, y: 0–1.5) were prepared, characterized by several physicochemical techniques (infrared [IR], scanning electron microscopy-energy dispersive X-ray [SEM/EDX], and ^{31}P nuclear magnetic resonance [NMR] spectroscopies, X-ray diffraction [XRD] diffraction, and thermogravimetric analysis [TGA]) and used as catalysts for the oxidation of cyclohexanone using hydrogen peroxide (30%) as an oxidant. The reaction products, AA, glutaric acid (GA), succinic acid (SA), hexanoic, 6-hydroxyhexanoic, 7,7-dimethoxy, and heptanoic acids and 1,1-dimethoxy octane were identified by gas chromatography–mass spectrometry (GC–MS) analysis. Only AA, GA, and SA were quantified by high-performance liquid chromatography (HPLC), the other products were noted X. The effects of POMs' counterion nature, molar ratios of catalyst/-one and cyclohexanone/cyclohexanol, and reaction time on the reaction product distribution were investigated. The used catalysts were analyzed by ^{31}P NMR. $H_1Mn_{0.25}Co_{0.75}PMo_{12}O_{40}$ catalytic stability was examined in five consecutive cycles.

2. Experimental section

2.1. Material synthesis

$H_3PMo_{12}O_{40}$ heteropolyacid (noted H_3PMo_{12}) was prepared according to the classical method described by Tsigdinos [41]. $H_{3-2(x+y)}Mn_xCo_y$ mixed heteropolysalts

were synthesized by a two-step cationic exchange [36,37,39] under the stochiometric conditions (x, y: 0–1.5). The first step consists of an exchange of protons of H_3PMo_{12} by Ba^{2+} ions according to Eq. (1). In the second step, Mn^{2+} and Co^{2+} ions replace those of Ba^{2+} that precipitates as $BaSO_4$, according to Eq. (2). $Ba(OH)_2$ was gradually dissolved in an aqueous solution of $H_3PMo_{12}O_{40}$, 4.8×10^{-2} M, to avoid a sharp increase in pH that will lead to the decomposition of Keggin anion. The pH must be maintained at <2. Then, both Mn and Co sulfates, according to the fixed stoichiometric coefficients, were added to the previous solution. The Ba^{2+} ions precipitate as $BaSO_4$. The $H_{3-2(x+y)}Mn_xCo_yPMo_{12}O_{40}$ soluble salts were separated from $BaSO_4$ by filtration and dried at 50 °C and the mixed salts recovered as a powder.

$$H_3PMo_{12}O_{40} + (x+y)\,Ba(OH)_2 \rightarrow H_{3-2(x+y)}Ba_{(x+y)}PMo_{12}O_{40} + 2(x+y)\,H_2O \quad (1)$$

$$H_{3-2(x+y)}Ba_{(x+y)}PMo_{12}O_{40} + x\,MnSO_4 + y\,CoSO_4 \rightarrow H_{3-2(x+y)}Mn_xCo_yPMo_{12}O_{40} + BaSO_4\downarrow \quad (2)$$

2.2. Characterization

The composition and the weight percentages of P, Mo, Co, and Mn in the samples were measured with EDX microanalysis (SEM/EDX) using a HITACHI S3400 N tungsten filament microscope, equipped with an X-ray microanalysis system. Before starting the process of analysis, the samples were covered with carbon to improve their conductivity. Following this procedure the metal content could be estimated within an experimental error of ±0.5%. SEM images were recorded using an ESEM xL30 microscope.

Thermal analysis was performed between room temperature and 600 °C, under airflow with a heating rate of 5 °C/min using a TGA 2050 apparatus.

IR spectroscopy (1200–400 cm^{-1}) was performed using a Nicolet 6700 Fourier transform infrared spectrometer (CsI), including an attenuated total reflectance (ATR) module with a diamond crystal.

XRD patterns were recorded at room temperature in the 2θ range between 2° and 60° with a Siemens D5000 diffractometer using copper anticathode Cu Kα (λ = 1.5418 Å) at 40 kV and 40 mA. The indexing of the diffraction lines and phase identification were performed using the EVA software including a high score database.

Solid-phase ^{31}P NMR spectroscopy was carried out at room temperature using a BioSpin GmbH, Bruker spectrometer, equipped with a probe of 3.2 mm in diameter (double mode). Eighty-five percent H_3PO_4 was used as an external reference.

2.3. Catalytic reaction

The cyclohexanone oxidation was carried out under reflux at 90 °C according to the literature [42]. The reaction principle is to oxidize the reactant by POM catalyst. A POM color change from yellow to green or to blue-green (characteristic color of Mo^V) was observed. Then, 0.5 ml of hydrogen peroxide (30%) was added to restore the oxidant state (VI) of Mo characterized by yellow color. This sequence is repeated after each color change until there is no more change of color. Depending on the nature of the catalytic system, the added volume of H_2O_2 can vary between 5 and 12 ml. The reaction end, indicating that the reactant was totally consumed, is observed, when the POM catalyst is no longer reduced. It is noteworthy that up to 90 °C, hydrogen peroxide may be decomposed. The preliminary tests showed that the AA formation did not take place when the reaction mixture is constituted either of substrate and catalyst only, or substrate, catalyst, and hydrogen peroxide simultaneously or in the absence of catalyst.

The homogeneous reaction mixture was analyzed by HPLC and GC–MS. HPLC was connected to a quaternary pump and a UV–vis detector (210 nm). HPLC (YL9100 HPLC) analysis was carried out on a Tracer Excel 120 ODSB-C18 phase (25 cm × 4.6 mm, 5 μm particle size) using a 30% methanol in 5 mM of ammonium acetate buffer (pH 3.3) at 30 °C with a flow rate of 1 ml/min. GC–MS analysis was carried out using a GC–MS (GC 6890 plus, MSD5973, Hewlett Packard-5MS) with HP-INNOWAX column (30 m × 0.25 mm). The mass analysis is of quadripole type (150 °C). Purified helium was used as the carrier gas with a flow rate of 0.5 ml/min. The injector temperature and injector volume were 250 °C and 0.2 μl. The split ratio was 20:1. The ionization source (electronic impact) temperature was kept at 230 °C and that of the interface at 280 °C.

Before catalytic test, hydrogen peroxide concentration was verified by potassium permanganate titration.

3. Results and discussion

3.1. Characterization results

The heteropolysalt chemical composition determined by SEM/EDX analysis is reported in Table 1. The stochiometric coefficients adjusted considering 12 Mo atoms per Keggin unit were found in good agreement with desired stoichiometries for the transition metal atom number (Mn and/or Co). These results show a good correlation between the experimental formula, deduced from SEM/EDX analysis, and theoretical one confirming thus the feasibility of the cationic exchange method used in this study.

TGA curves of the samples (not represented here) show different mass losses. The first loss of ca. 9–12% was observed in the temperature range 50–180 °C, corresponding to the departure of 8–13 hydration water molecules. The second one of ca. 1–3% observed in the range 180–380 °C was attributed to the departure of constitution water molecules that results from the combination of protons with oxygen atoms of Keggin anion. Above 400 °C, the POM decomposition to P_2O_5, MoO_3, MnO, and CoO occurred. TGA results are reported in Table 2. A good correlation between experimental and theoretical formulas was observed, confirming also the reliability of the cationic exchange synthesis method.

The XRD patterns registered for $H_1Mn_{0.25}Co_{0,75}$ and $H_1Mn_{0.75}Co_{0,25}$ with $(x+y) = 1$ (Fig. 1) are similar to that of H_3PMo_{12} acid that crystallizes in a triclinic system [43].

Table 1
Elemental analysis of $H_{3-2(x+y)}Mn_xCo_y$ heteropolysalts obtained by SEM/EDX analysis.

$H_{3-2(x+y)}Mn_xCo_y$	Composition (Wt %)				Molar ratio		
	P	Mo	Mn	Co	P	Mn	Co
$H_1Mn_{0.25}Co_{0.75}$	7.60	84.95	1.80	5.65	1.07 (1)	0.25 (0.25)	0.79 (0.75)
$H_1Mn_{0.75}Co_{0.25}$	7.17	84.92	5.73	2.16	1.01 (1)	0.80 (0.75)	0.30 (0.25)
$H_0Mn_{0.75}Co_{0.75}$	7.74	81.83	5.32	5.11	1.13 (1)	0.78 (0.75)	0.74 (0.75)
$H_0Mn_{1.50}Co_{0.00}$	6.91	81.75	11.33	/	1.01 (1)	1.66 (1.50)	/

( ) Theoretical values; / absence.

Table 2
Thermal analysis results of $H_{3-2(x+y)}$ Mn_xCo_y solids.

Theoretical formula	TGA deduced formula	Hydration water molecules
$H_{3.00}Mn_{0.00}Co_{0.00}$	$H_{2.98}Mn_{0.00}Co_{0.00}$	8
$H_{0.00}(Mn\ Co)_{1.50}$	$H_{0.06}(Mn\ Co)_{1.47}$	12
$H_{1.00}(Mn\ Co)_{1.00}$	$H_{0.96}(Mn\ Co)_{1.02}$	11
$H_{1.00}(Mn\ Co)_{1.00}$	$H_{0.94}(Mn\ Co)_{1.03}$	15
$H_{0.00}Mn_{1.50}Co_{0.00}$	$H_{0.02}Mn_{1.49}Co_{0.00}$	13
$H_{0.00}Mn_{0.00}Co_{1.50}$	$H_{0.06}Mn_{0.00}Co_{1.43}$	13

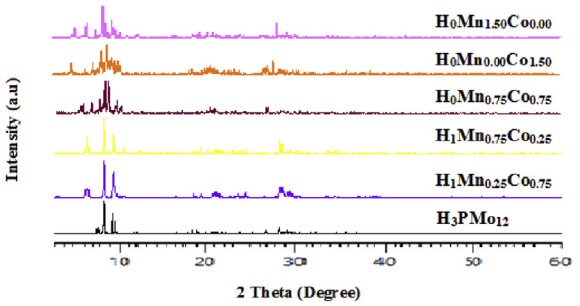

Fig. 1. XRD patterns of $H_{3-2}(x + y)Mn_xCo_y$ solids.

In the absence of proton ($x + y = 1.5$), $H_0Mn_0Co_{1.5}$, $H_0Mn_{0.75}Co_{0.75}$, and $H_0Mn_{1.5}Co_0$ crystallize in a quadratic system (high score database) [44].

The Fourier transform infrared data of POMs, presented in Table 3, show the characteristic vibration frequencies of phosphorus–oxygen and metal–oxygen bonds of Keggin anion in the spectral range 1100–600 cm^{-1} [45]. Asymmetric stretching phosphorus–oxygen bond, ν_{as} P–O_a, was observed at 1060 cm^{-1} and those of metal–oxygen, ν_{as} Mo–O_d, ν_{as} Mo–O_b–Mo, and ν_{as} Mo–O_c–Mo, at 962–955, 895–879, and 791–785 cm^{-1} respectively. For $x + y = 1.5$, the vibration frequency values of salts are close to those obtained with H_3PMo_{12} acid, whereas for $x + y = 1$ ($H_1Mn_{0.25}Co_{0.75}$ and $H_1Mn_{0.75}Co_{0.25}$) a small shoulder at around 978 cm^{-1} was observed on Mo=O_d vibration bond. This latter is very sensitive to the Keggin anion symmetry because of its high charge density induced by the presence of both cobalt and manganese ions.

Table 3
IR vibration wave numbers (cm^{-1}) of $H_{3-2(x+y)}Mn_xCo_y$.

$H_{3-2(x+y)}Mn_xCo_y$		ν (P–O_a)	ν (M=O_b)	ν (M–O_b–M)	ν (M–O_c–M)
X	Y				
0.00	0.00	1058	955	879	785
0.25	0.75	1060	962 (980)[a]	879	791
0.75	0.25	1060	958 (978)[a]	879	787
1.50	0.00	1060	957	889	789
0.75	0.75	1060	957	893	791
0.00	1.50	1060	957	889	789

[a] Shoulder.

It is known that ^{31}P NMR analysis is very sensitive to the local chemical environment and surrounding symmetry of phosphorus atom in the Keggin unit. Solid-state ^{31}P NMR data (Table 4) of $H_1Mn_{0.25}Co_{0.75}$, $H_1Mn_{0.75}Co_{0.25}PMo_{12}$, $H_0Mn_{0.75}Co_{0.75}$, and $H_0Mn_{1.5}Co_0$ salts show chemical shifts at −4.33, −4.50, −4.30, and −4.16 ppm, respectively, values close to that of H_3PMo_{12} (−4.4 ppm), suggesting the same phosphorus atom environment, evidencing thus the purity of samples. The small difference in the chemical shift is because of the proton substitution degree of H_3PMo_{12} by Mn and/or Co.

The SEM images show that the POM morphology is sensitive to its chemical composition (Fig. 2). H_3PMo_{12} shows a very porous texture whereas $H_0Mn_0Co_{1.5}$, $H_1Mn_{0.25}Co_{0.75}$, and $H_0Mn_{0.75}Co_{0.75}$ show a compact texture constituted of aggregates of irregular particle sizes and for $H_0Mn_{1.5}Co_0$, an assembly of small groups of crystals separated by voids leading to a nonhomogeneous texture.

3.2. Catalytic performances of $H_{3-2(x+y)}Mn_xCo_y$

The catalytic properties of Keggin-type mixed salts, $H_{3-2(x+y)}Mn_xCo_y$, were examined in the liquid-phase oxidation of cyclohexanone (-one) and of mixture of cyclohexanone and cyclohexanol (-ol/-one) in the presence of hydrogen peroxide (30%) at 90 °C.

The GC–MS analysis obtained with $H_1Mn_{0.25}Co_{0.75}$ are given as an example and results are presented in Table 5. The results show, in addition to the formation of AA and GA, that of following acids: hexanoic, 6-hydroxyhexanoic, and 7,7-dimethoxy heptanoic acids and 1,1-dimethoxy octane. The presence of both 6-hydroxyhexanoic and hexanoic acids was already observed for the Baeyer–Villiger oxidation of cyclohexanone [46,47]. It is

Table 4
^{31}P NMR data of $H_{3-2(x+y)}Mn_xCo_y$ compounds.

POM	δ (ppm)
H_3PMo_{12}	−4.40
$H_0Mn_{0.75}Co_{0.75}$	−4.30
$H_1Mn_{0.25}Co_{0.75}$	−4.33
$H_1Mn_{0.75}Co_{0.25}$	−4.50
$H_1Mn_{1.50}Co_0$	−4.16

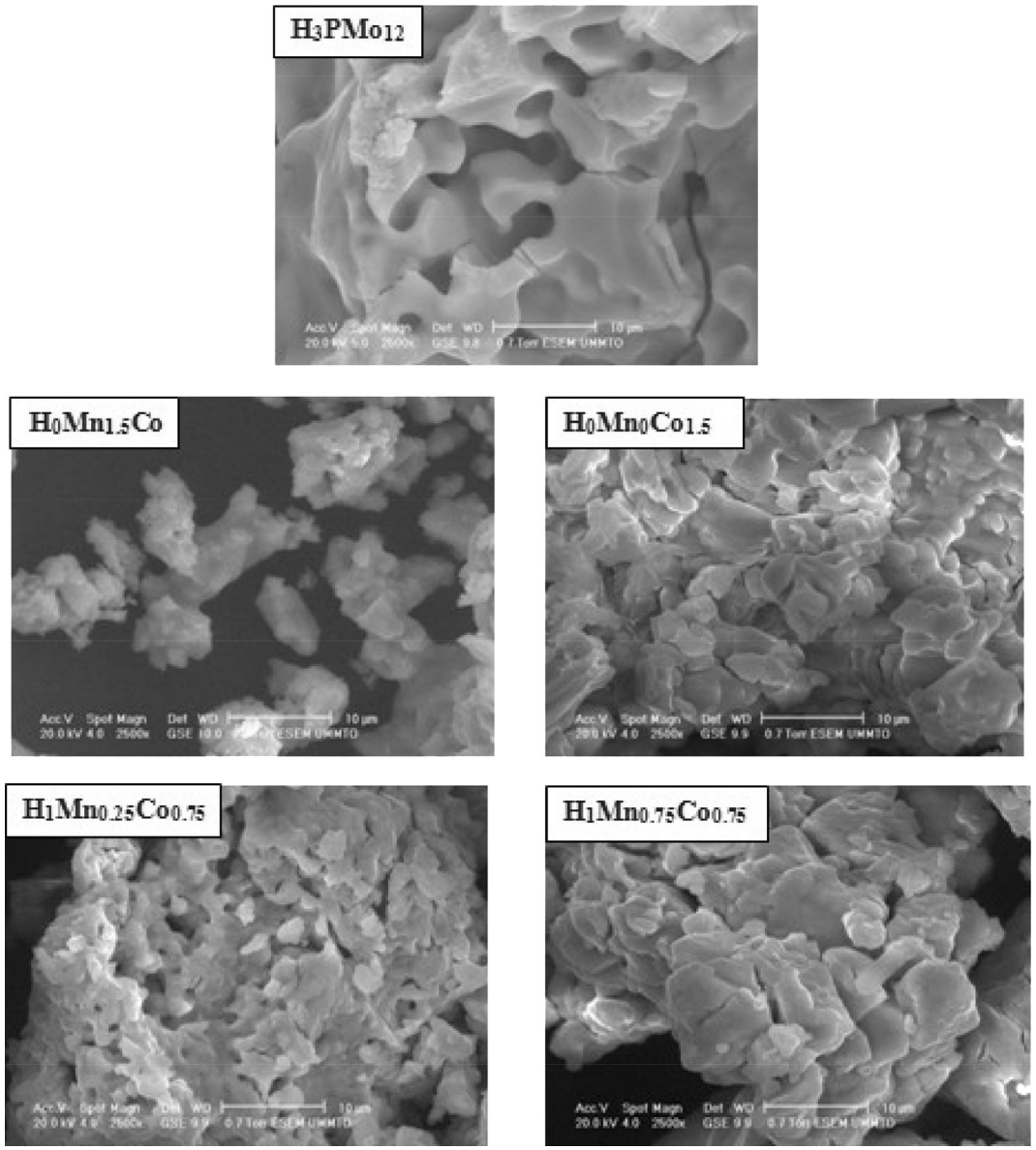

Fig. 2. SEM images of $H_{3-2(x+y)}Mn_xCo_y$.

noted that SA was observed with other systems. In this study, onlyAA, SA, and GA were quantified by HPLC, the other products were noted X.

3.2.1. Cyclohexanone oxidation

To optimize the reaction conditions, H_3PMo_{12} was used as a catalyst for the oxidation of cyclohexanone. The obtained results are the following: a catalyst/-one molar ratio of 0.47×10^{-3} corresponding to a catalyst mass of 0.03 g and substrate amount of 30 mmol, a reaction time of 20 h, and an agitation rate of 1000 rpm.

In this study, the effects of POM counterion nature, molar ratios of catalyst/-one and cyclohexanone/cyclohexanol, and reaction duration on the reaction product distribution were examined.

3.2.1.1. Effect of POM counterion nature. As shown in Table 6, the catalytic systems are very active with 96–100% of cyclohexanone conversion. AA and X are the major reaction products observed with selectivities varying between 41-66% and 29–51%, respectively. GA was obtained with selectivities inferior to 10%. Except for $H_1Mn_{0.75}Co_{0.25}$ system, the introduction of both Mn and Co favors the AA formation, evidencing the positive effect of the partial substitution of H_3PMo_{12} protons by these elements. Thus, AA yields are of 56–64% against 46% for H_3PMo_{12}. Among substituted systems, $H_1Mn_{0.25}Co_{0.75}$ is the best catalyst, with an AA yield reaching 64%.

3.2.1.2. Effect of catalyst/-one molar ratio. The effect of catalyst/-one molar ratio was performed with $H_1Mn_{0.25}$

Table 5
Results of GC–MS analysis obtained in the presence of $H_1Mn_{0.25}Co_{0.75}$.

Retention time (min)	Product name	Formula	Molar mass (g/mol)
06.78	Hexanoic acid	$C_6H_{12}O_2$	116
07.96	6-Hydroxyhexanoic acid	$C_6H_{12}O_3$	132
08.43	AA (by removal of two methyl groups)	$C_6H_{10}O_4$	146
08.94	7,7-Dimethoxyheptanoic acid	$C_9H_{18}O_4$	190
09.18	AA (by removal of a single methyl group)	$C_6H_{10}O_4$	146
09.40	Thiohexanoic acid, s-butyl ester	$C_{10}H_{20}OS$	188
09.55	1,1-Dimethoxyoctane	$C_{10}H_{22}O_2$	174

Conditions: T_{react}, 90 °C; m_{cat}, 0.18 g; n_{-one}, 30 mmol; agitation rate, 1000 rpm; H_2O_2, 0.5 ml; and $t = 20$ h.

$Co_{0.75}$, the most efficient catalyst. The cyclohexanone conversion and reaction product selectivities are reported in Fig. 3. Regardless the value of catalyst/-one molar ratio, the cyclohexanone conversion is total, thus confirming the high activity of catalyst. A catalyst/-one molar ratio of 2.84×10^{-3} leads to the highest AA selectivity (77%) and to the lowest X selectivity (20%). With catalyst/-one molar ratios superior to 2.84×10^{-3}, AA selectivity gradually decreases from 77% to 38% whereas that of X increases from 20% to 47%. The highest SA selectivity (20%) was obtained with a catalyst/n-one molar ratio of 4.26×10^{-3} whereas GA was practically not observed.

3.2.1.3. Effect of reaction time. Fig. 4 shows the reaction time effect on the cyclohexanone conversion and reaction product selectivities in the presence of $H_1Mn_{0.25}Co_{0.75}$ catalyst. Each time reaction corresponds to a catalytic test. With a time reaction of 10 h, the cyclohexanone conversion attains more than 95%. The distribution of reaction products is sensitive to the reaction duration. Thus, in 10 h of reaction, X selectivity reached the maximum (71%) and that of AA the minimum (27%). Although within 20 h, the selectivity of AA attains the maximum (77%) and that of X the minimum (22%). Within 25 h of reaction, AA and X selectivities are of 52% and 35%, respectively. From these results, it can be concluded that in 20 h of reaction some X products could act as intermediates for AA formation and within 25 h of the reaction, AA could decompose and thus favor the formation of some compounds X. The HPLC chromatogram (Fig. 5) shows the distribution of the reaction products after 20 h of reaction. The formation of both GA and SA varies little with the duration of the reaction. A reaction time of 20 h, necessary to obtain the highest AA yield, has already been reported in our previous work [36–40] as well as by other authors [46,47].

Table 6
Effect of $H_{3-2(x+y)}Mn_xCo_y$ composition on cyclohexanone oxidation conversion and reaction product selectivities (yields).

POM	Conversion (%)	Selectivities (yields) (%)			X
		AA	GA	SA	
H_3PMo_{12}	100	46 (46)	3 (3)	0 (0)	51 (51)
$H_0Mn_{0.75}Co_{0.75}$	96	58 (56)	9 (9)	0 (0)	33 (31)
$H_1Mn_{0.25}Co_{0.75}$	97	66 (64)	5 (5)	0 (0)	29 (28)
$H_1Mn_{0.75}Co_{0.25}$	98	41 (40)	8 (8)	0 (0)	51 (50)
$H_2Mn_{0.25}Co_{0.25}$	100	58 (58)	7 (7)	0 (0)	35 (35)

Reaction conditions: T_{react}, 90 °C; catalyst/-one molar ratio, 0.47×10^{-3}; agitation rate, 1000 rpm; mode addition of the oxidant, 0.5 ml; and reaction time, 20 h.
X, Unidentified products.
AA, adipic acid.
AG, glutaric acide.
As, succenic.

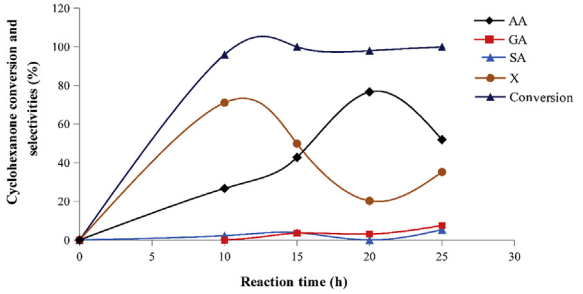

Fig. 3. Cyclohexanone conversion and reaction product selectivities as a function of catalyst/-one molar ratio. Catalyst, $H_1Mn_{0.25}Co_{0.75}$; T_{react}, 90 °C; agitation rate, 1000 rpm; and reaction time, 20 h.

3.2.2. Cyclohexanone/cyclohexanol mixture oxidation

In the case of cyclohexanone/cyclohexanol mixture oxidation, only AA recovered by crystallization was considered. The reaction was examined over $H_1Mn_{0.25}Co_{0.75}$ with a catalyst/(ol + one) molar ratio of 2.84×10^{-3}. The catalytic results (Fig. 6) show a gradual decrease in AA yield from 75% to 0% when the percentage of added alcohol increases from 0 to 100. Similar results are already reported [48–53]. The oxidation of alcohol took place (a color change in catalyst was observed) but the AA formation was not observed. The negative effect of the alcohol addition can be attributed to the formation of hydrogen bond between the C=O group of the ketone and the hydrogen of C–OH group of the cyclohexanol, which makes difficult the oxidation of cyclohexanone. Therefore, alcohol inhibits the AA formation.

The series $H_{3-2(x+y)}Mn_xCo_yPMo_{12}O_{40}$ showed its efficiency in the oxidation of cyclohexanone, exhibiting high catalytic performances that can be explained by their dissolution in the reaction medium, thus making all of the catalytic sites more accessible to the substrate. The efficiency of cobalt- and manganese-based catalysts was already reported by other authors for the oxidation of cyclohexane by molecular oxygen. This efficiency was attributed to the existence of redox couples, Mn^{IV}/Mn^{III} and Co^{III}/Co^{II} [54]. Molybdenum-based POMs are also known for their high oxidative power associated with the high oxidation state of the molybdenum (Mo^{VI}) [55–58]. In the presence of elements as Co^{II}, Sn^{II}, and Sb^{III}, the polyanion, $[PMo_{12}O_{40}]^{3-}$, can easily be reduced, thus leading to partial reduced POM with coexistence of several elements with different oxidation states as in our case $H_{3-2}(Mn^{IV}/Mn^{II})_x(Co^{III}/Co^{II})_yP(Mo^{VI}/Mo^{V})_{12}O_{40}$. This was obtained during its preparation confirmed by its blue color. Partial reduced POMs are known as “heteropoly-blue”. This aspect can facilitate the electron transfer during the oxidation of cyclohexanone.

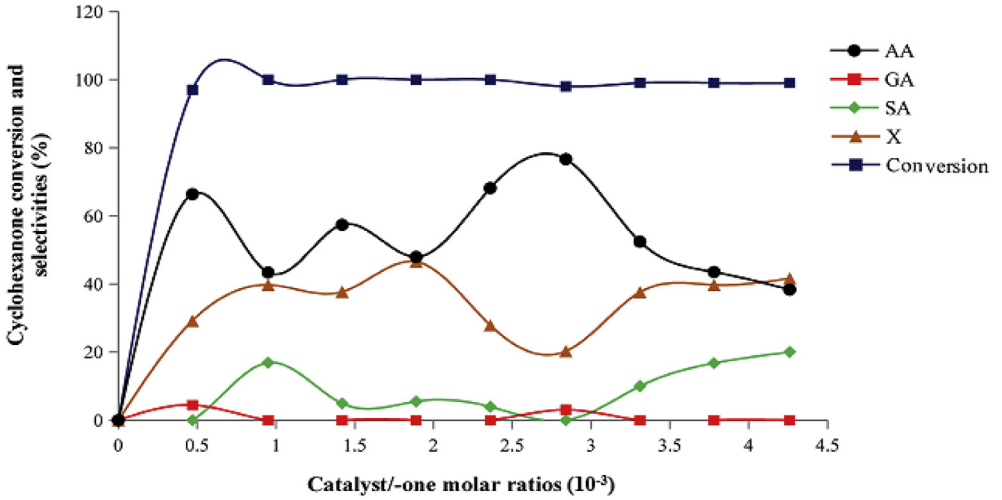

Fig. 4. Cyclohexanone conversion and reaction product selectivities as a function of reaction time. Catalyst, $H_1Mn_{0.25}Co_{0.75}$; T_{react}, 90 °C; agitation rate, 1000 rpm; and catalyst/-one molar ratio, 2.83×10^{-3}.

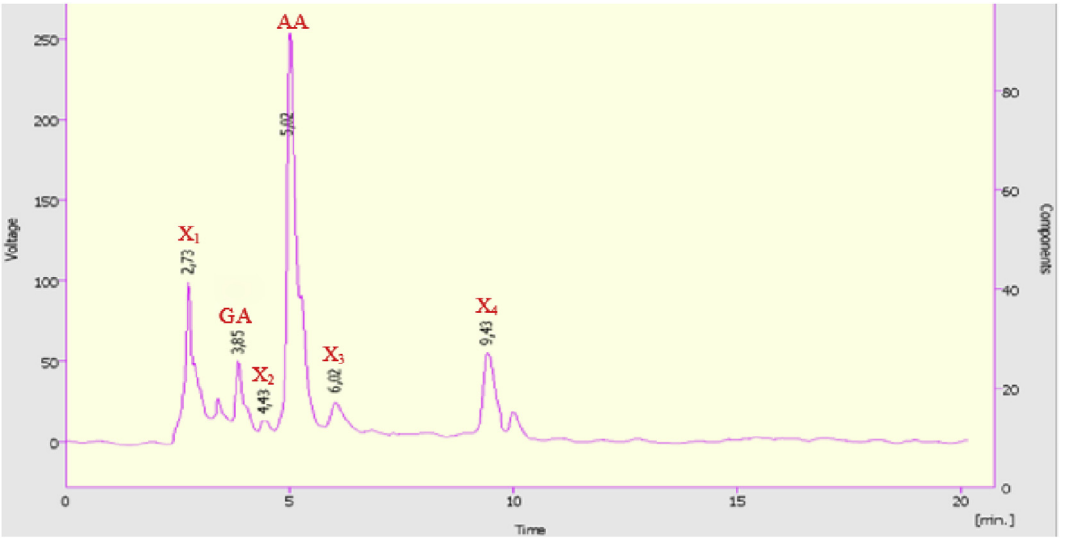

Fig. 5. HPLC chromatogram of obtained mixture in the presence of $H_1Mn_{0.25}Co_{0.75}$. Catalyst, $H_1Mn_{0.25}Co_{0.75}$; T_{react}, 90 °C; catalyst/-one molar ratio of 2.84×10^{-3}; agitation rate, 1000 rpm, reaction time, 20 h.

Among the tested systems, the best catalytic performance was obtained by the formulation, $H_1Mn_{0.25}Co_{0.75}$, that exhibited an AA yield of 75%, which was higher than those obtained with Keggin and Dawson series [36–40] and lower than those obtained from the oxidation of cyclohexane and cyclohexene (80–90%) [59–62]. Its effectiveness may be related to the presence of the proton that can accelerate the cyclohexanone molecule activation through a ketonic–enolic tautomer equilibrium, thus leading to the 2-hydroxy cyclohexanone formation in a first step [63]. In a second step, the system consisting of several redox couples, Mn^{IV}/Mn^{II}, Co^{III}/Co^{II}, and Mo^{VI} in Mo^{V}, formed from a partial reduction of Mo^{VI} to Mo^{V} during the catalyst preparation would lead to several different peroxo species, after the addition of hydrogen peroxide. These peroxo species, in turn, could oxidize and provide oxygen atoms to the reaction intermediates, leading to the final products., among which AA.

3.2.3. Catalyst stability

To examine the $H_1Mn_{0.25}Co_{0.75}$ catalyst stability, five cycles of oxidation reaction were performed. After the first cycle that lasted 20 h, the AA was recovered after cold crystallization and then 30 mmol of cyclohexanone was added to the filtrate and the oxidation reaction was renewed under the same experimental conditions. Fig. 7

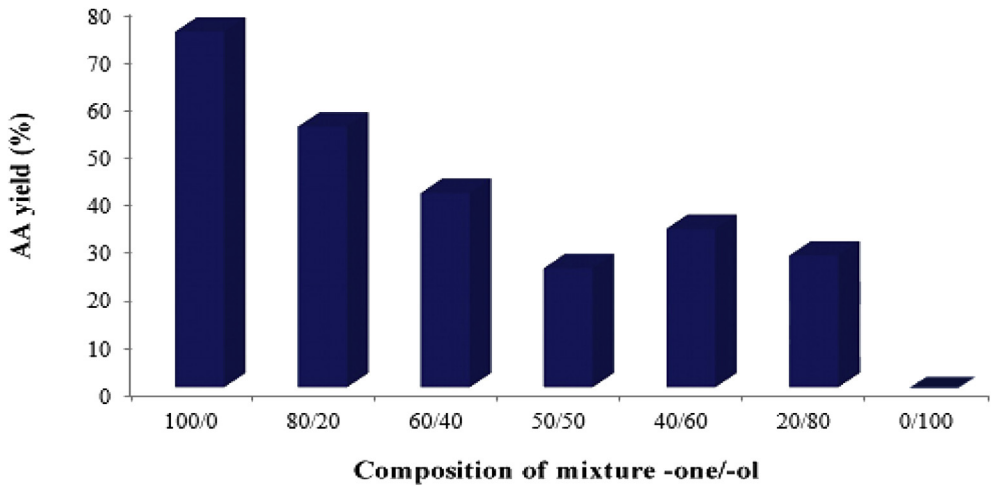

Fig. 6. AA yield as a function of the composition of mixture -one/-ol. Catalyst, $H_1Mn_{0.25}Co_{0.75}$; T_{react}, 90 °C; agitation rate, 1000 rpm; catalyst/-one molar ratio, 2.83×10^{-3}.

shows that the AA yield gradually decreases from 61% to 0%. It can be suggested that this yield decrease is due to following parameters: (1) the salt acidity decreases after each reduction of H_2O_2, oxidant needing the presence of the protons, and (2) the reaction medium comes more diluted resulting from the H_2O_2 reduction to water.

3.2.4. Characterization of the used catalyst

The used catalysts were analyzed by ^{31}P NMR after 20 h of reaction. Table 7 shows that they exhibit several peaks evidencing phosphorus-based species formation. The chemical shifts were observed at −3.14 and −5.5 ppm for H_3PMo_{12}, −3.75 and −6.89 ppm for $H_0Mn_{0.75}Co_{0.75}$, and −3.76, −6.19, −6.84, and −12.94 ppm for $H_1Mn_{0.25}Co_{0.75}$. These values are different from that of the oxidized specie, $[PMo_{12}O_{40}]^{3-}$ (−4.30 to −4.40 ppm). It was reported that in the presence of hydrogen peroxide, the POM was broken down into several species identified by ^{31}P NMR as peroxo species. In the case of the $H_3PW_{12}O_{40}$, the species are $\{PO_4[WO(O_2)_2]_4\}^{3-}$ and $\{PO_4[WO(O_2)_2]_2\}^{2-}$ [64–68]. From these observations, it can be assumed that the peroxo-POM species could be the active species for the formation of carboxylic acids.

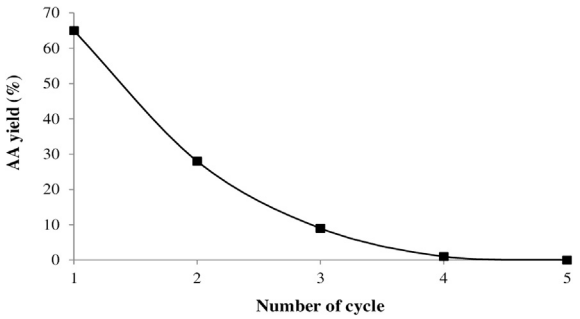

Fig. 7. AA yield variation as a function of cycle number. Catalyst, $H_1Mn_{0.25}Co_{0.75}$; T_{react}, 90 °C; catalyst/-one molar ratio, 2.84×10^{-3}; agitation rate, 1000 rpm; reaction time, 20 h.

3.2.5. Oxidation reaction pathways

For the cyclohexanone oxidation process in the presence of $H_{3-2(x+y)}Mn_xCo_y$ catalysts, several steps were evidenced: (1) oxidation of the substrate confirmed by a color change of catalyst from yellow, characteristic color of Mo^{VI} species (POMox) to blue, characteristic color of Mo^{V} species (POMred), involving a Mars and Van Krevelen type mechanism in which the oxygen atoms of the crystalline lattice participate in the oxidation process (Eq. 3); (2) oxidation of POMred to POMox by H_2O_2 (a color change from blue to yellow) with simultaneously the peroxo-POM formation as revealed by ^{31}P NMR analysis (Eq. 4), and (3) the peroxo-POM species can react with some products from Eq. 3 that could be the intermediates to form the carboxylic acids whose AA (Eq. 5). By analogy with the explanation of Eq. 3 (Mars and Van Krevelen mechanism), the peroxo-ions (O_2^{2-}) of the peroxo-POM would intervene in the oxidation. It was also reported that the peroxo-POM was considered as an electrophilic agent, which would produce an electrophilic attack on the oxygen atom of the intermediate specie, generating then the corresponding carboxylic acid as observed in the case of sulfide oxidation by H_2O_2 on POMs [69].

$$\text{Cyclohexanone} + \text{POMox} \rightarrow \text{POM}_{red} + \text{products} + \text{intermediates} \quad (3)$$

$$H_2O_2 + \text{POM}_{red} \rightarrow \text{peroxo} - \text{POM}_{ox} \quad (4)$$

Table 7
Results of ^{31}P NMR analysis of different POMs before and after cyclohexanone oxidation.

POM	δ (ppm) before reaction	δ(ppm) after reaction
H_3PMo_{12}	−4.40	−3.14/−5.52
$H_0Mn_{0.75}Co_{0.75}$	−4.30	−3.75/−6.89
$H_1Mn_{0.25}Co_{0.75}$	−4.33	−3.76/−6.19/−6.84/−12.94

$$\text{Peroxo} - \text{POM}_{ox} + \text{intermediatespecies} \rightarrow \text{reactionproducts} + \text{POMox} \quad (5)$$

4. Conclusions

In this study, a series of Keggin-type POMs of formula $H_{3-2(x+y)}Mn_xCo_yPMo_{12}O_{40}$ was prepared, characterized, and tested in homogeneous oxidation reactions of cyclohexanone and cyclohexanol/cyclohexanone mixture using H_2O_2 as an oxidant.

Physicochemical analysis has confirmed the formulation of $H_{3-2(x+y)}$ Mn_xCo_y with $x + y = 3/2$ and x, y: 0–1.5, thus demonstrating the feasibility of the used cationic exchange method.

The catalytic results showed that all studied systems are very active in the cyclohexanone oxidation (conversions >95%) that leads to several products as AA, GA, SA, hexanoic, 6-hydroxyhexanoic, and 7,7-dimethoxy, and heptanoic acids and 1,1-dimethoxy octane, identified by GC–MS. Among reaction products (AA, GA, and SA) quantified by HPLC, AA is the major product for following reaction conditions: a catalyst/substrate molar ratio of 2.84×10^{-3} and 20 h of reaction. With a composition of $H_1Mn_{0.25}Co_{0.75}$, the AA yield attains the maximum (75%). The peroxo-POM species could be the active species for the formation of carboxylic acids from products coming from the first step, substrate oxidation by POM.

The use of $H_{3-2(x+y)}Mn_xCo_y$ as catalysts, hydrogen peroxide as an oxidant without addition of a solvent, leads to clean and efficient process that may be an alternative to that using the harmful, toxic, and corrosive nitric acid.

Appendix A. Supplementary data

Supplementary data related to this article can be found at https://doi.org/10.1016/j.crci.2019.01.003.

References

[1] S. Van de Vyver, Y. Román-Leshkov, Catal. Sci. Technol. 31 (2013) 1465–1479.
[2] Y. Wu, C. Cordier, E. Berrier, N. Nuns, C. Dujardin, P. Granger, Appl. Catal. B Environ. 140–141 (2013) 151–163.
[3] D. Pietrogiacomi, M.C. Campa, L.R. Carbone, S. Tuti, M. Occhiuzzi, Appl. Catal. B Environ. 187 (2016) 218–227.
[4] A.V. Leont'ev, O.A. Fomicheva, M.V. Proskurnina, N.S. Zefirov, Russ. Chem. Rev. 70 (2001) 91–104.
[5] J. Pérez-Ramıırez, F. Kapteijn, K. Schöffel, J.A. Moulijn, Appl. Catal. B Environ. 44 (2003) 117–151.
[6] S. Ghosh, S.S. Acharyya, S. Adak, L.N. Sivakumar- Konathala, T.S.R. Bal, Green Chem. 16 (2014) 2826–2834.
[7] S.S. Acharyya, S. Ghosh, R. Bal, Green Chem. 17 (2015) 3490–3499.
[8] B.M. Trost, I. Fleming, in: S.V. Ley (Ed.), Comprehensive Organic Synthesis, Pergamon Press, Oxford, 1991, p. 251.
[9] J.R. Holum, Org. Chem. 26 (1961) 4814.
[10] J.C. Collins, W.W. Hess, F.J. Frank, Tetrahedron Lett. 9 (1968) 3363.
[11] E.J. Corey, J.W. Suggs, Tetrahedron Lett. 16 (1975) 2647.
[12] R.J. Highet, W.C. Wildman, J. Am. Chem. Soc. 77 (1955) 4399.
[13] D.G. Lee, U.A. Spitzer, Org. Chem. 35 (1970) 3589.
[14] R.V. Stevens, K.T. Chapman, H.N. Weller, Org. Chem. 45 (1980) 2030.
[15] B. Sarkar, P. Prajapati, R. Tiwari, R. Tiwari, S. Ghosh, S.S. Acharyya, C. Pendem, R.K. Singha, L.N.S. Konathala, J. Kumar, T. Sasaki, R. Bal, Green Chem. 14 (2012) 2600–2606.
[16] J.H. Tong, L.L. Bo, Z. Li, Z.Q. Lei, C.G. Xia, Mol. Catal. A Chem. 73 (2009) 58–63.
[17] P.R. Makgwane, S.S. Ray, Catal. Commun. 54 (2014) 118–123.
[18] L.P. Zhou, J. Xu, H. Miao, F. Wang, X.Q. Li, Appl. Catal. A 292 (2005) 223–228.
[19] A. Selvamani, M. Selvaraj, M. Gurulakshmi, R. Ramya, K. Shanthi, J. Nanosci, Nanotechnology 14 (2014) 2864–2870.
[20] M. Zabihi, F. Khorasheh, J. Shayegan, RSC Adv. 5 (2015) 5107–5122.
[21] J. Li, Y. Shi, L. Xu, G.Z. Lu, Ind. Eng. Chem. Res. 49 (2010) 5392–5399.
[22] Y. Fu, W.C. Zhan, Y. Guo, Y.Q. Wang, X.H. Liu, Y. Guo, Y.S. Wang, G.Z. Lu, Microporous Mesoporous Mater. 214 (2015) 101–107.
[23] R. Zhao, Y.Q. Wang, Y.L. Guo, Y. Guo, X.H. Liu, Z.G. Zhang, Y.S. Wang, W.C. Zhan, G.Z. Lu, Green Chem. 8 (2006) 459–466.
[24] J. Li, X. Li, Y. Shi, D.S. Mao, G.Z. Lu, Catal. Lett. 137 (2010) 180–189.
[25] L.P. Zhou, J. Xu, H. Miao, X.Q. Li, F. Wang, Catal. Lett. 99 (2005) 231–234.
[26] T. Iwahama, K. Syojyo, S. Sakaguchi, Y. Ishii, Org. Process Res. Dev. 2 (1998) 255–260.
[27] M. Wu, W. Zhan, Y. Guo, Y. Guo, Y. Wang, L. Wang, G. Lu, Appl. Catal. A Gen. 523 (2016) 97–106.
[28] R. Ishimoto, K. Kamata, N. Mizuno, Angew. Chem. Int. Ed. 121 (2009) 9062.
[29] K. Kamata, M. Kotani, K. Yamaguchi, S. Hikichi, N. Mizuno, Chem. Eur. 13 (2007) 639.
[30] A. Troupis, T.M. Triantis, E. Gkika, A. Hiskia, E. Papaconstantinou, Appl. Catal. B Environ. 86 (2009) 98–107.
[31] D. Sloboda-Rozner, P.L. Alsters, R. Neumann, J. Am. Chem. Soc. 125 (2003) 5280.
[32] J. Wang, L. Yan, G. Li, X. Wang, Y. Ding, J. Suo, Tetrahedron Lett. 46 (2005) 7023.
[33] S. Pathan, A. Patel, Appl. Catal. A 459 (2013) 59.
[34] F.M. Menger, C. Lee, Org. Chem. 44 (1979) 3446.
[35] M.M.Q. Simoes, C.M.M. Conceiao, J.A.F. Gamelas, P.M.D.N. Domínguez, A.M.V. Cavaleiro, J.A.S. Cavaleiro, A.J.V. Ferrer-Correira, R.A.W. Johnstone, Mol. Catal. A Chem. 144 (1999) 461–468.
[36] T. Mazari, S. Benadji, A. Tahar, L. Dermeche, C. Rabia, Mater. Sci. Eng. B. 3 (2013) 146–152.
[37] A. Tahar, S. Benadji, T. Mazari, L. Dermeche, C. Marchal-Roch, C. Rabia, Catal. Lett. 145 (2015) 569–575.
[38] L. Mouheb, L. Dermeche, T. Mazari, S. Benadji, N. Essayem, C. Rabia, Catal. Lett. 148 (2) (2018) 612–620.
[39] S. Benadji, T. Mazari, L. Dermeche, N. Salhi, E. Cadot, C. Rabia, Catal. Lett. 143 (2013) 749–755.
[40] M. Moudjahed, L. Dermeche, S. Benadji, T. Mazari, C. Rabia, Mol. Catal. A Chem. 414 (2016) 72–77.
[41] G.A. Tsigdinos, Ind. Eng. Chem. Prod. Res. Dev. 13 (1974) 267–274.
[42] K. Nomiya, M. Miwa, Y. Sugaya, Polyhedron 3 (1984) 607–610.
[43] H. Copaux, Ann. Chim. 17 (1909) 217.
[44] L.M. Rodriguez-Albelo, G. Rousseau, P. Mialane, J. Marrot, C. Mellot-Draznieks, A.R. Ruiz-Salvador, S. Li, R. Liu, G. Zhang, B. Keita, A. Dolbecq, Dalton Trans. 41 (2012) 9989–9999.
[45] C. Rocchiccioli-Deltcheff, M. Fournier, R. Franck, R. Thouvenot, Mol. Struct. 114 (1984) 49.
[46] F. Cavani, K. Raabova, F. Bigi, C. Quarantelli, Chem. Eur. 16 (2010) 12962–12969.
[47] Y. Usui, K. Sato, Green Chem. 5 (2003) 373–375.
[48] A.F. Lindsay, Chem. Eng. Sci. 8 (1954) 78–93.
[49] A. Castellan, J.C.J. Bart, S. Cavallaro, Catal. Today 9 (1991) 255.
[50] A. Castellan, J.C.J. Bart, S. Cavallaro, Catal. Today 9 (1991) 285.
[51] A. Castellan, J.C.J. Bart, S. Cavallaro, Catal. Today 9 (1991) 301.
[52] F. Kapteijn, J. Rodriguez-Mirasol, J.A. Moulijn, Appl. Catal. B Environ. 9 (1996) 25.
[53] S.A. Chavan, D. Srinivas, P. Ratnasamy, J. Catal. 39 (2002) 39.
[54] M. Wu, W. Zhan, Y. Guo, Y. Guo, Y. Wang, L. Wang, G. Lu, Catalysts 7 (2017) 155.
[55] C. Marchal-Roch, N. Laronze, N. Guillou, A. Tézé, G. Hervé, Appl. Catal. A 203 (2000) 143–150.
[56] C. Marchal-Roch, N. Laronze, N. Guillou, A. Tézé, G. Hervé, Appl. Catal. A 199 (2000) 33–44.
[57] T. Mazari, C. Marchal-Roch, S. Hocine, N. Salhi, C. Rabia, J. Nat. Gas Chem. 19 (2010) 54–60.
[58] F. Jing, B. Katryniok, F. Dumeignil, E. Bordes-Richard, S. Paul, J. Catal. 309 (2014) 121–135.
[59] P. Blach, Z. Böstrom, S. Franceschi-Messant, A. Lattes, E. Perez, I. Rico-Lattes, Tetrahedron Lett. 66 (2010) 7124–7128.
[60] I. Quesada-Penate, G. Lesage, P. Cognet, M. Poux, Chem. Eng. J. 202 (2012) 357–364.
[61] J. Alcaniz-Monge, G. Trautwein, A. Garcia-Garcia, Mol. Catal. A Chem. 394 (2014) 211–216.

[62] M. Shang, T. Noël, Q. Wang, Y. Su, K. Miyabayashi, V. Hessel, S. Hasebe, Chem. Eng. J. 260 (2015) 454–462.
[63] D. Amitouche, M. Haouas, T. Mazari, S. Mouanni, R. Canioni, C. Rabia, E. Cadot, C. Marchal-Roch, Appl Catal. A 561 (2018) 104–116.
[64] (a) P. Mars, D.W. Van-Krevelen, Chem. Eng. Sci. 3 (1954) 41–59; (b) C.N. Satterfield, Heterogeneous Catalysis in Practice, 2nd ed., McGraw-Hill, New York, 1980.
[65] L. Salles, C. Aubry, R. Thouvenot, F. Robert, C. Doremieux-Morin, G. Chottard, H. Ledon, Y. Jeanin, P. Bregault, Inorg. Chem. 33 (1994) 871–878.
[66] D.C. Ducan, C. Chamber, E. Hecht, C.L. Hill, J. Am. Chem. Soc. 117 (1995) 681–691.
[67] L.I. Kuznetsova, N.I. Kuznetsova, R.I. Maksimovskaya, G.I. Aleshina, O.S. Koscheeva, U.V. Utkin, Catal. Lett. 141 (10) (2011) 1442.
[68] L.Y. Mengs, S.R. Zhai, Z.C. Sun, F. Zhang, Z.Y. Xiao, Q.D. An, Microporous Mesoporous Mater. 204 (2015) 123.
[69] R. Frenzel, Á.G. Sathicq, M.N. Blanco, G.P. Romanelli, L.R. Pizzio, Mol. Catal. A Chem. 403 (2015) 27–36.